Impacts of building layout on pedestrian level wind comfort and gas pollutant diffusion

Yi Yang, Tianxiao Zhang, Haiying Xie*, Xiaoxiao Wang

Department of Environmental Science and Engineering, University of Shanghai for Science and Technology, Shanghai 200093, P R China

ARTICLE INFORMATION

CORRESPONDING AUTHOR:

xiehy@usst.edu.cn
Tel: (0086 21)55271991
Fax: (0086 21)55271991

ABSTRACT

Introduction: The impacts of building layout on pedestrian level wind comfort and gas pollutant diffusion are simulated using computational fluid dynamics method.

Materials and methods: The control equations of flow and pollutant diffusion are solved by using ANSYS Fluent. The SIMPLE algorithm is selected for the pressure-velocity coupling. The data from wind tunnel experiment at Tokyo Polytechnic University is employed in the validation case.

Results: The velocity field and turbulence intensity at pedestrian level under different building layouts are obtained. The distribution and evaluation of wind comfort grade and pollutant concentration are given.

Conclusion: Building layouts have significant impacts on flow and pollutant diffusion at pedestrian level. The outward staggered layout of building group can improve both wind comfort grade and air quality, but the inward staggered layout has the adverse effect. Non-staggered layouts are the worst in terms of the wind comfort grade in this paper.

Introduction

The high-rise buildings in urban areas block the wind at high altitude and lead its kinetic energy down to the ground, which sometimes causes uncomfortable wind environment for pedestrians [1–6]. Numerous studies were focused on the discomfort conditions caused by the strong wind at pedestrian level and the measures of reducing wind speed such as modification of building corner and selecting appropriate orientation and building layout [4, 7].

However, in the muggy and humid summer of tropical and sub-tropical areas, moderate wind speed is necessary for pedestrian thermal comfort [8–10]. The effects of lift-up design on the improvement of the low wind conditions at pedestrian level were numerically investigated [8, 9]. At the same time, air pollution such as traffic pollutants also cannot diffuse under low wind conditions [11–14]. In densely built-up cities, many factors such as building height, roof shape, and balcony have impacts on pollutant dispersion near ground [15–19]. Therefore, it is necessary to achieve an appropriate wind speed

at pedestrian height for both wind comfort and good air quality.

In fact, building layout plays an important role in influencing flow fields near buildings [5, 11]. In previous studies on this issue, pollutant diffusion and wind comfort were rarely considered simultaneously. This work aims to discuss the impact of building layout on wind comfort and gas pollutant diffusion together, and give the optimum building layouts that can meet the requirements of pedestrian level wind comfort and be conducive to air pollutant diffusion.

To obtain the characteristics of wind environment and pollutant diffusion around buildings, computational fluid dynamics (CFD) method has been widely used for its advantages of low cost and short time-using [20–22]. It generally applies the finite volume method to solve the fluid continuity, momentum and species transport equations. CFD method gives basically satisfactory results in both the wind field simulation of regular and irregular buildings and the simulation of ideal and real urban pollutant diffusion [5, 6, 11]. Because the flow around buildings is mostly turbulent, an appropriate turbulence model should be selected [23].

Materials and methods

Equations of flow and pollutant diffusion

Eqs. 1 and 2 are the conservation laws of mass and momentum for the steady air flow around buildings.

$$\frac{\partial(\rho u_i)}{\partial x_i} = 0 \tag{1}$$

$$\frac{\partial(\rho u_i u_j)}{\partial x_j} = -\frac{\partial p}{\partial x_i} + \frac{\partial}{\partial x_j}\left(\mu \frac{\partial u_i}{\partial x_j} - \rho \overline{u'_i u'_j}\right) \tag{2}$$

Where x_j and u_j are the coordinate component and velocity component in the j direction, p is the pressure, μ is the fluid kinematic viscosity, and

ρ is the fluid density, $-\rho \overline{u'_i u'_j}$ is the turbulent stress. When the influence of sunshine on air temperature is not considered, ρ can be taken as a constant.

Eq. 3 gives the expression of turbulent stress,

$$-\rho \overline{u'_i u'_j} = \mu_t \left(\frac{\partial u_i}{\partial x_j} + \frac{\partial u_j}{\partial x_i}\right) - \frac{2}{3}\rho k \delta_{ij} \tag{3}$$

Where k is the turbulent kinetic energy, μ_t is the turbulent viscosity coefficient.

To solve μ_t in Eq. 3, the standard k-ε turbulence model is used to describe the turbulence effect. Eqs. 4 and 5 are the transport equations of k and ε, in which ε stands for the turbulent energy dissipation rate. Thus μ_t can be obtained by using Eq. 6.

$$\frac{\partial(\rho u_j k)}{\partial x_j} = \frac{\partial}{\partial x_j}\left[\left(\mu + \frac{\mu_t}{\sigma_k}\right)\frac{\partial k}{\partial x_j}\right] + G_k - \rho\varepsilon \tag{4}$$

$$\frac{\partial(\rho u_j \varepsilon)}{\partial x_j} = \frac{\partial}{\partial x_j}\left[\left(\mu + \frac{\mu_t}{\sigma_\varepsilon}\right)\frac{\partial \varepsilon}{\partial x_j}\right] + C_{\varepsilon 1}\frac{\varepsilon}{k}G_k - C_{\varepsilon 2}\rho\frac{\varepsilon^2}{k} \tag{5}$$

$$\mu_t = \rho C_\mu \frac{k^2}{\varepsilon} \tag{6}$$

Where, G_k represents the generation of turbulence kinetic energy, $C_{\varepsilon 1}$, $C_{\varepsilon 2}$ and C_μ are empirical constants, σ_k and σ_ε are the turbulent Prandtl numbers for k and ε. In addition to the standard k-ε model, RNG k-ε, standard k-ω and SST k-ω models are also used in the following simulations and the detailed description of these models can be found in Ref. [24].

When there is no chemical reaction in the air, gas pollutants can be considered as passive scalars. The governing equation of pollutant concentration distribution is expressed by:

$$\frac{\partial}{\partial x_j}\left(\rho u_j Y_P\right) = \frac{\partial}{\partial x_j}\frac{\partial Y_P}{\partial x_j}\left(\rho D_{P,m} + \frac{\mu_t}{Sc_t}\right) + S_P \tag{7}$$

Where Y_P is the concentration of pollutant P, S_P is the pollutant emission rate, $D_{P,m}$ is the molecular diffusion coefficient of pollutant P, Sc_t is the turbulent Schmidt number, μ_t/Sc_t represents pollutant diffusion due to turbulence.

Simulation method and settings

ANSYS ICEM is used to discretize the computational domain. Due to the regular shape of the building and domain, the structured grid is adopted and refined near the places where flow changes dramatically such as grounds and building walls. The mesh size of the first layer near the wall is taken as about 1-2% of the building height. In solving the control equations of flow and pollutant diffusion with ANSYS Fluent, the SIMPLE algorithm is selected for the pressure-velocity coupling and convection terms are discretized by using the second-order upwind scheme. The criterion for judging the iterative convergence is that the scaled residuals for all equations are less than 10^{-5}.

Model validation

Geometry and settings

Based on the experiment of a single-block building at the wind tunnel of Tokyo Polytechnic University [25], a validation model was built as shown in Fig. 1. Flow and concentration fields around the building are numerically simulated. The reliability of the selected computation model and method is validated according to the agreement between the simulated results and experimental data.
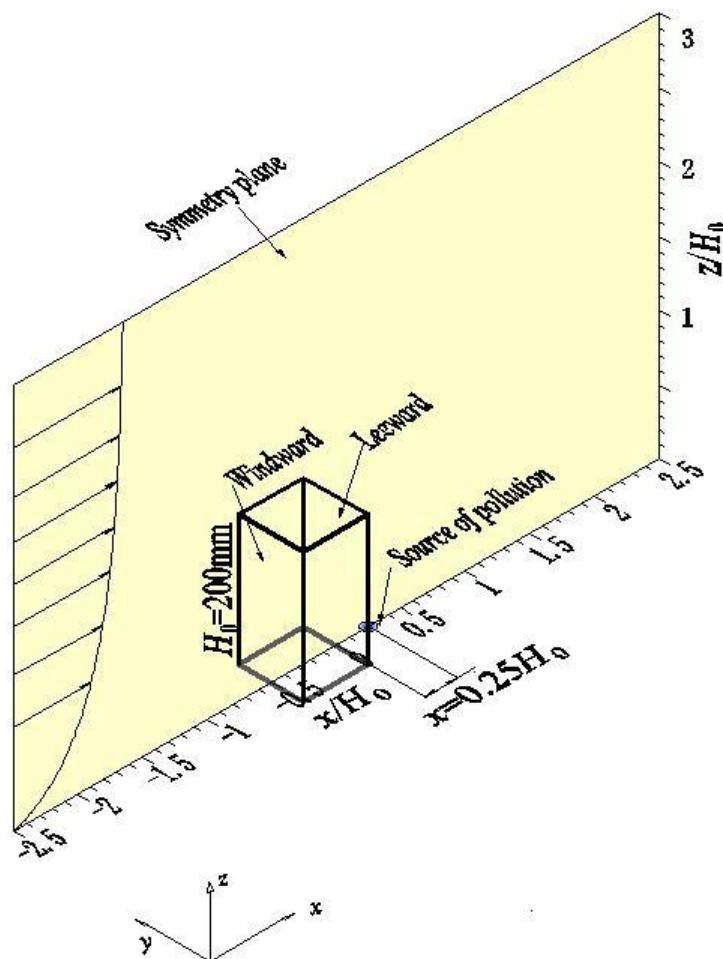
Fig. 1. Geometry of the building and point source [25]

As shown in Fig. 1, the rectangular building is 0.2 m in height (H_0) and 0.1 m in both length and width. Ethylene is selected as pollutant, which is released outward from the point source set on the ground and 0.25 H_0 away from the leeward of the building. Experimental results of velocity and pollutant concentration at 4 lines on the symmetry plane (y=0) are chosen in model validation. The 4 lines are right behind the building and named as line-x-H_0-0.125, line-x-H_0-0.25, line-x-H_0-0.5 and line-x-H_0-1.0 respectively. The name line-x-H_0-0.125 represents the line is 0.125 H_0 away from the leeward of the building, and the positions of other three lines can be determined in the same way.

The computational domain setting (shown in Fig. 2) conforms to the CFD guidelines [26]. The total number of mesh is approximately 2.5 million. According to the wind tunnel experiment, the domain inlet velocity is given as:

$$u = U_r(z/H_0)^{0.25} \qquad (8)$$

Where Ur=4.2m/s. The turbulent intensity at the domain inlet is given as piece-wise functions which are obtained by fitting the experimental data. The outlet face is set as an outflow condition. All walls are set as non-slip conditions. In addition, the two lateral sides and top surface are all specified as symmetry conditions. When using the standard k-ε model and RNG k-ε model, the region near wall is treated by the standard wall function.
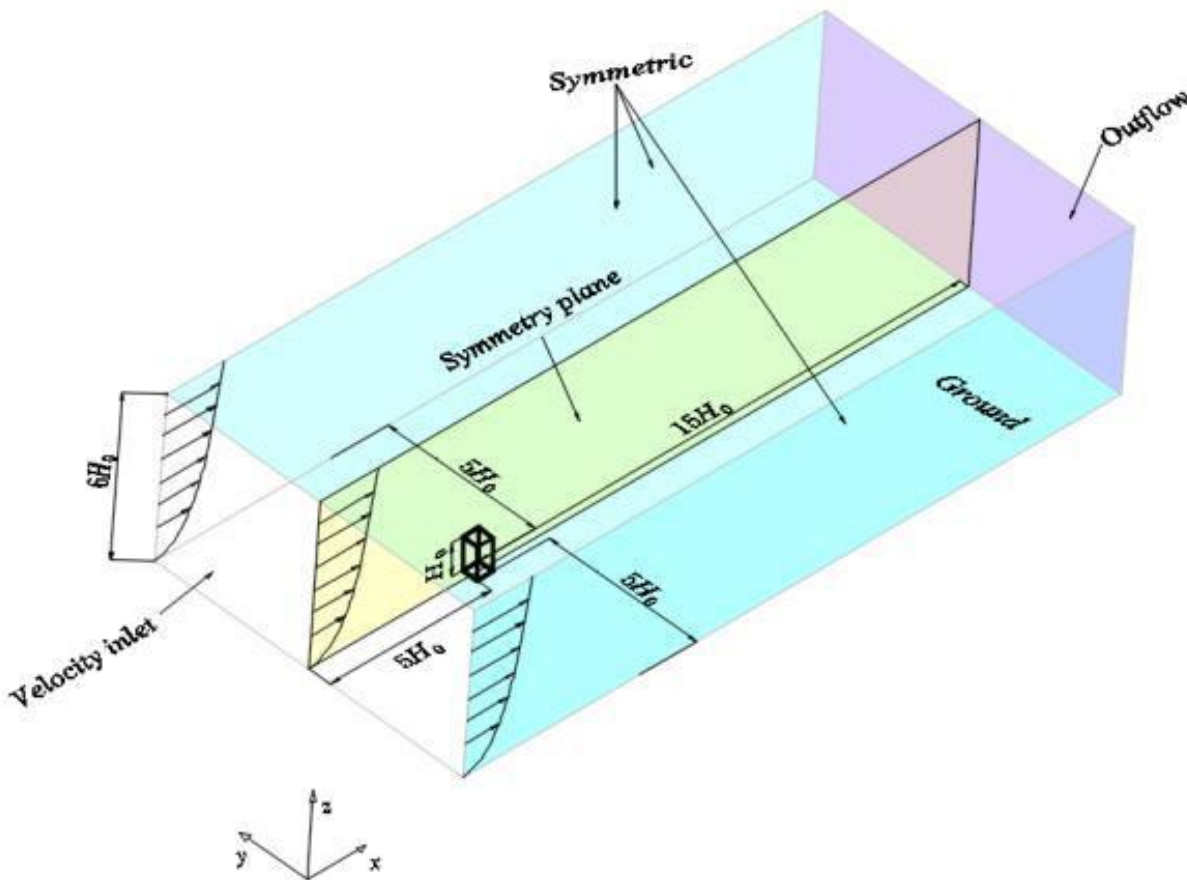
Fig. 2. Schematic of computational domain size and boundary conditions

Flow field validation

Fig. 3 shows the comparison of the vertical wind velocity between CFD simulation results and the experimental data at 4 lines on the symmetry plane. Standard k-ε model, RNG k-ε model, standard k-ω model and SST k-ω model are adopted in simulation. Fig. 4 shows that the performance of the standard k-ω model is not good, especially at line-x-H_0-0.25. At the positions with $z/H_0 > 0.8$, the simulation results

of the other three models are basically the same and all maintains good agreement with the experimental data. However, with the increase of x-coordinate value, the predicted velocity near the ground is smaller than the experimental value, which is also reported in the study by some researchers [11]. Generally the standard k-ε model performs better in consistency with the experimental values than RNG k-ε and SST k-ω models.
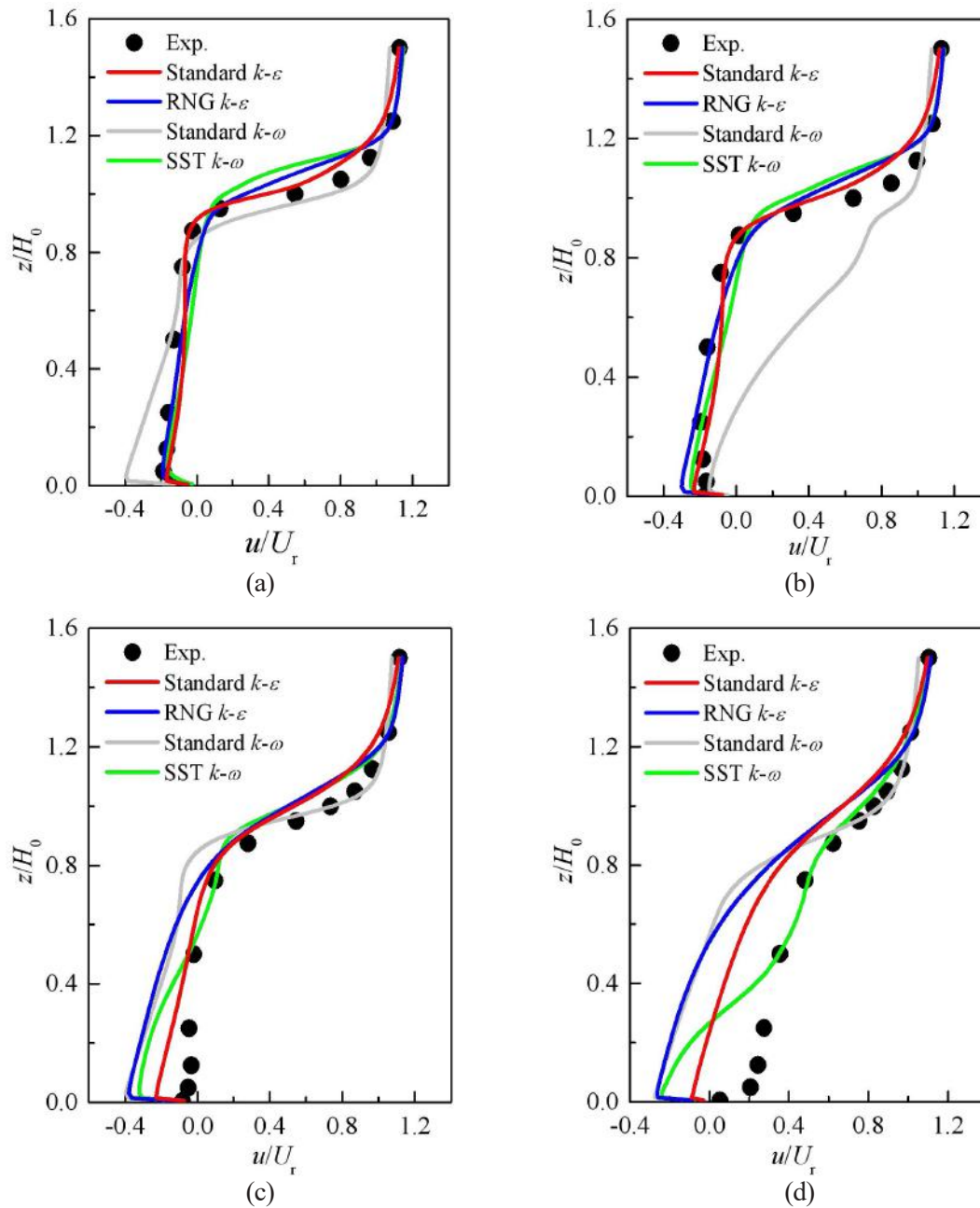
Fig. 3. Comparison of the velocity between CFD simulation results and experimental data: (a) line-x-H_0-0.125, (b) line-x-H_0-0.25, (c) line-x-H_0-0.5, (d) line-x H_0-1.0

Fig. 4 shows the streamline and velocity distribution on the symmetry plane (y=0) and the horizontal plane with z/H=0.25 using the standard k-ε model. Obviously the standard k-ε model is capable of predicting the main characteristics of the flow around the bluff body.

The above analysis shows that the standard k-ε model is a fast and accurate choice for CFD simulations of wind flow near the building. Therefore, the pollutant concentration field discussed next is obtained on the basis of the flow field with the standard k-ε model.

Concentration field validation

The turbulent Schmidt number is set as 0.7 in simulating the concentration field. Fig. 5 depicts the comparison between the simulated pollutant concentration results and the experimental data at positions of line -x-H_0-0.125, line-x-H_0-0.25, line-x-H_0-0.5 and line-x-H_0-1.0. In Fig.5 the normalized concentration K is used to indicate pollutant accumulation around the building. K is defined as:
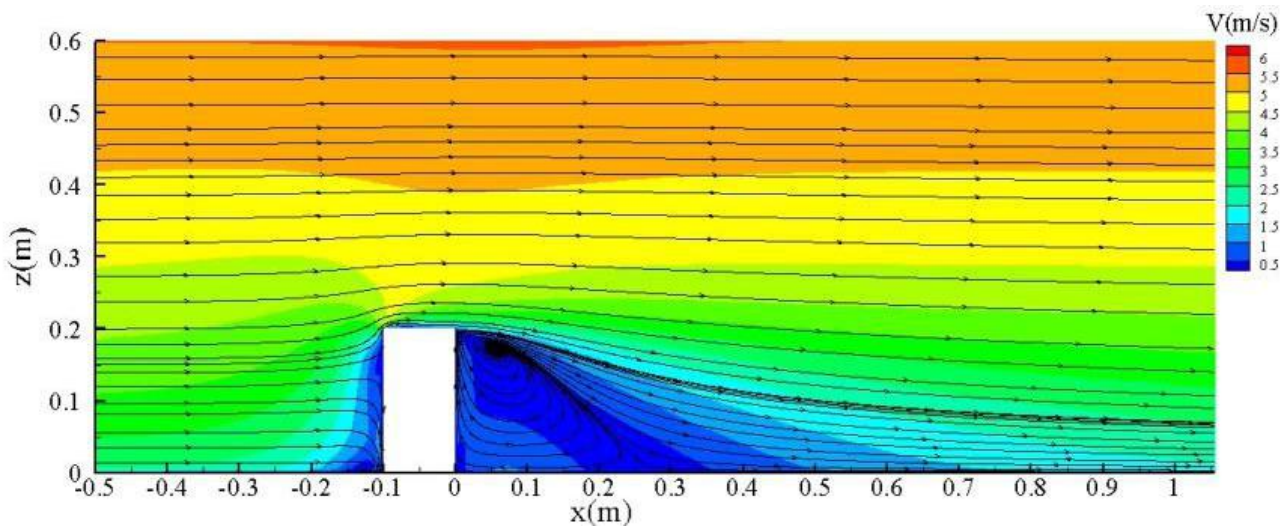
(a)
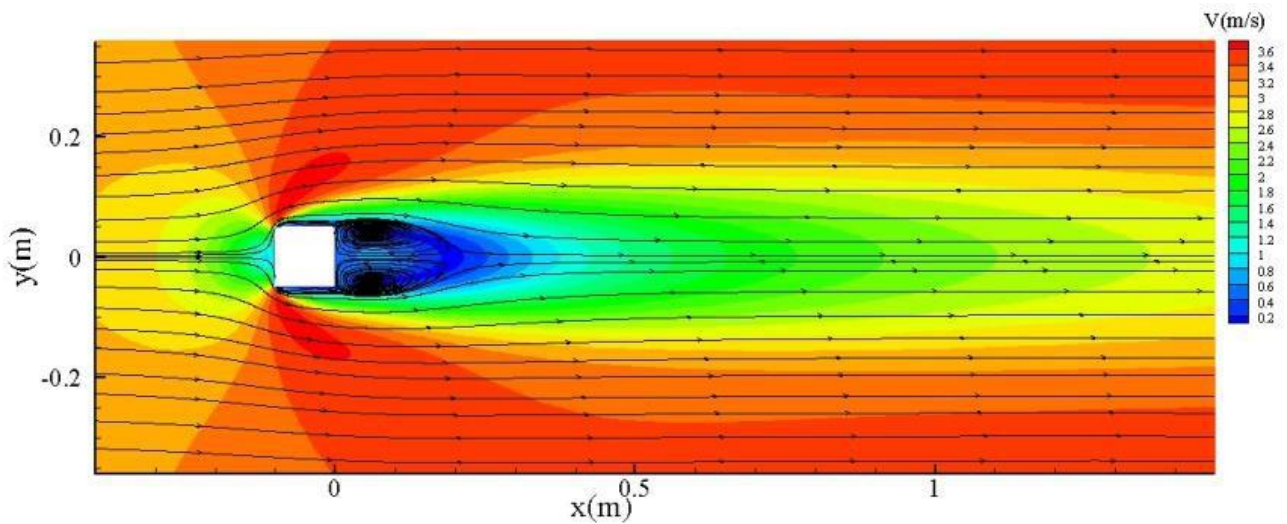
(b)

Fig. 4. Streamline and velocity distribution on the symmetry plane and horizontal plane: (a) y=0, (b) z/H = 0.25

$$K = c/C_0 \quad\quad\quad (9)$$

where c is the volume fraction of pollutant (ethylene), and C_0 is the reference emission concentration. According to the experiment [25], C_0 is defined as $c_{gas}\ q/u_{H0}H_0^2$, in which q is the flow rate (5.83×10^{-6} m³/s) of the mixture of ethylene and air released and c_{gas}, the ethylene concentration, is 1.0×10^6 ppm.

Since the ground source is $0.25\ H_0$ away from the leeward side of the building, the pollutants released are transported to the building by the

backflow close to the ground (see Fig. 4(a)), resulting in high K values at lower height of line-*x*-H_0-0.125 and line-*x*-H_0-0.25 (Fig 5(a) and (b)). The K decreases rapidly at the positions of line-H_0-0.5 and line-*x*-H_0-1.0 (Fig.5(c) and (d)). As illustrated in Fig. 5, the K values simulated agree well with the experimental data at positions with $z/H_0 > 0.5$. In the upstream positions of the source, the K values at locations close to the ground are also consistent with the observed values.
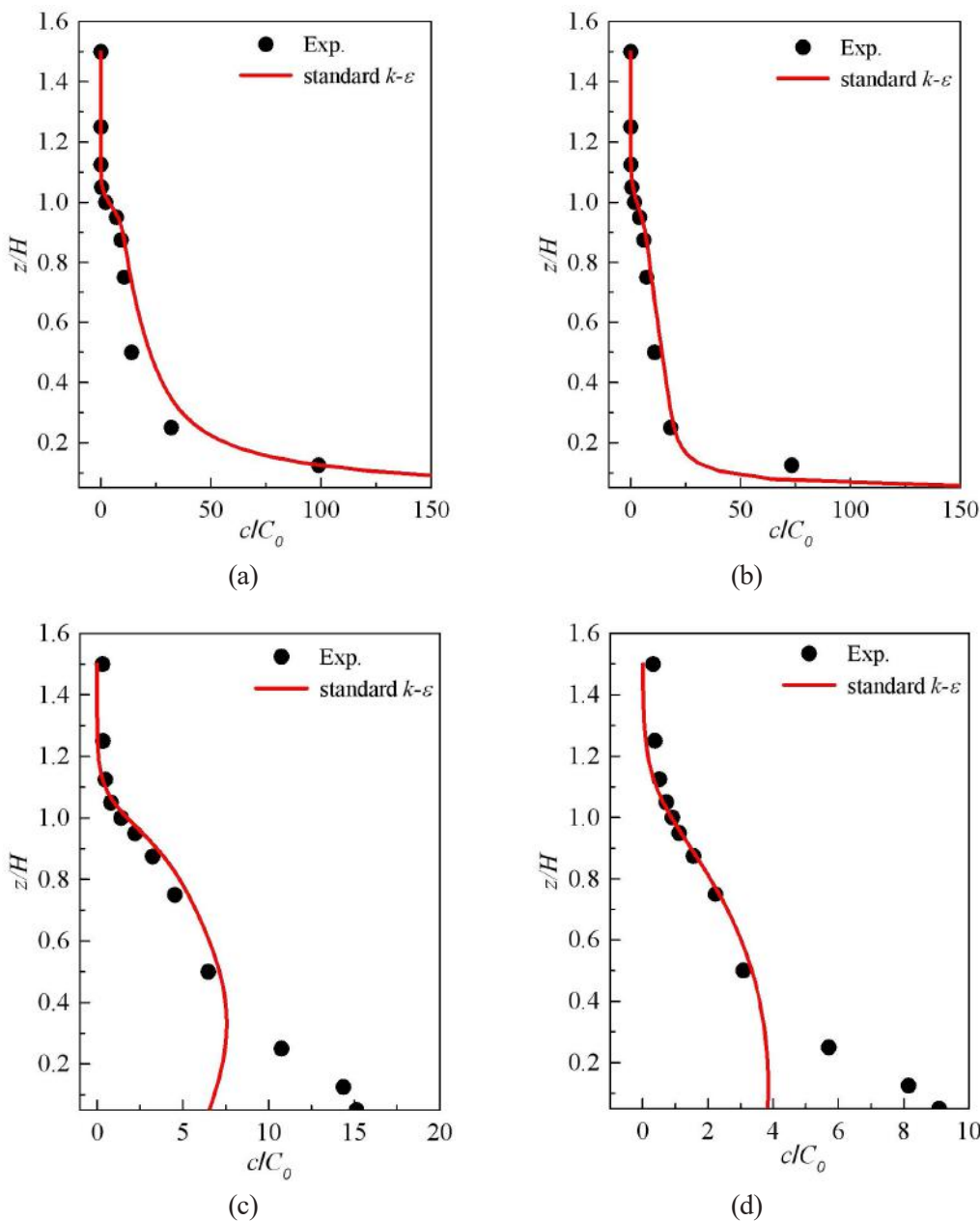
Fig. 5. Comparison of the concentration between CFD simulation results and experimental data: (a) line -x-H_0-0.125, (b) line-x-H_0-0.25, (c) line-x-H_0-0.5, (d) line-x H_0-1.0

However, at positions with $z/H_0<0.2$ of line -x-H_0-0.5 and line-x-H_0-1.0, the simulated K is about one half of the experimental value (Fig.5(c) and (d)). The discrepancy could be explained by the flow distribution in Fig. 4 (c) and (d). The simulated u is negative at positions with $z/H_0<0.2$ of line-x-H_0-0.5 and line-x-H_0-1.0, meaning that the flow here inhibits the convective transmission of pollutants from the source and resulting in lower values of K. In fact, the experimental u at the positions is positive, although u is very small. It is evident that the positive u can transport the pollutant downstream, resulting in relatively higher values of K. The underestimation of concentration predicted especially at positions with low pollutant levels has also been reported in literatures [11, 27], but it seems that no clear explanation has been provided.

In general, the simulated concentration data obtained by the standard k-ε model accord well with the experimental values.

Impacts of building layout on flow and pollutant diffusion

Building group geometries and settings

The layout of real urban building group is usually irregular and complex in shape, so it is difficult to determine the key factors and clarify their impacts on the flow and dispersion patterns. Therefore, this paper discusses the simplified regular layout of building groups shown in Fig. 6. The group is composed of 54 identical rectangular buildings, 6 rows and 9 columns in total. The length L, width W, height H and building interval D of the buildings are all 30m. The area surrounded by the red line is the target area with 3 columns upstream and 2 columns downstream. The setting of the traffic pollution source refers to the research by Hang [15]. Carbon monoxide (CO) is selected as pollutant, which is released from the source zone next to the target area (see Fig. 6). the source zone is 2 m high, and emission rate (M_0) is 1×10^{-7}kg/m³·s。
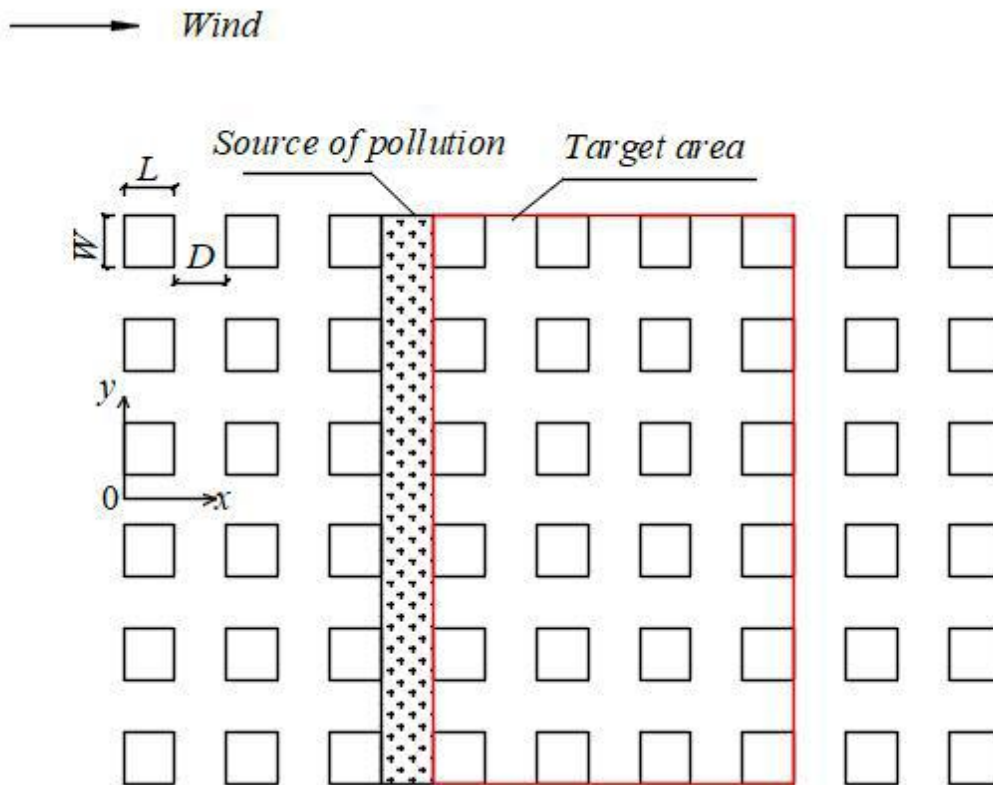
Fig. 6. Schematic of building layout

The computational domain is designed similarly as that of the validation case (see Fig. 7). The inlet, side and top surfaces of the domain are 5 H away from the peripheral boundary of the building group, and the outlet surface is 15 H away from the last column of buildings. Due to the symmetrical features of the flow, one half of the domain is taken to save the computational resources. Each building in the target area is named as B_{ij}, where i is the number of columns and j is the number of rows. Referring to the layout shown in Fig. 7, this paper also designs other four types of layout and the buildings outside the target area remains unchanged. Fig. 8 illustrates the layout designs, names and grid distributions around the buildings.

Case A and case E are of the same type with no buildings staggered. The open space in Case E is used for public activities. The other three types are staggered in different ways. For Case B, the second column B_{2j} moves inward by 0.5 W in –y direction while the third column B_{3j} moves outward by 0.5 W in +y direction. In Case C, B_{2j} and B_{4j} are translated with the same distance and direction as B_{2j} and B_{3j} in Case B. Then in Case D, B_{2j}, B_{3j} and B_{4j} are shifted outward by 0.5 W, 1.0 W and 1.5 W respectively in +y direction.

For the staggered cases, the computational domain size is almost the same as that of the non-staggered cases, but the lateral sides extend 5 H from the outermost building of the target area. In simulation, the standard k-ε model is selected. The boundary conditions and other settings are consistent with those of the validation case.
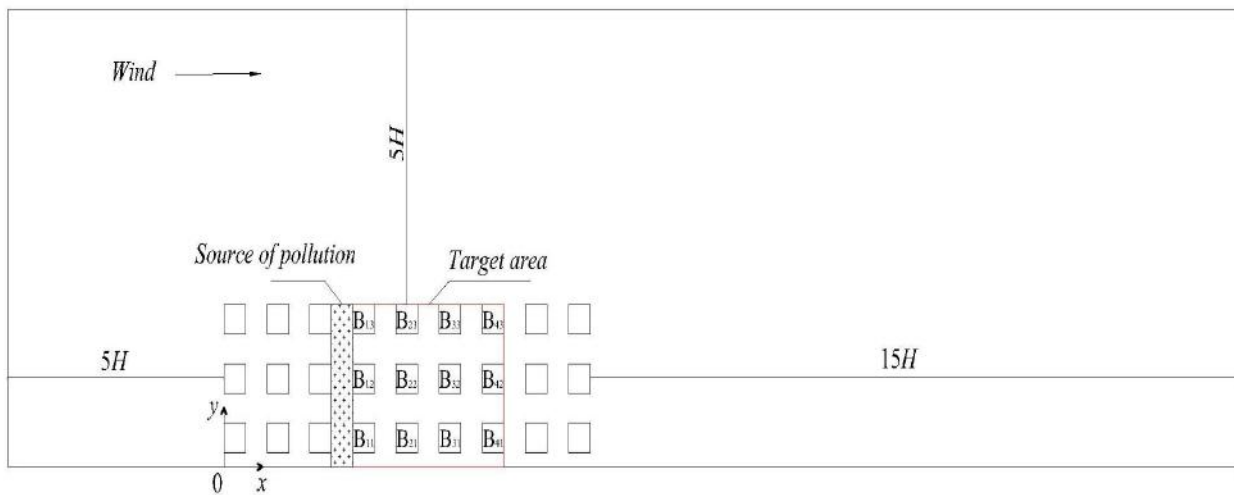
Fig. 7. Schematic of computational domain settings for building group
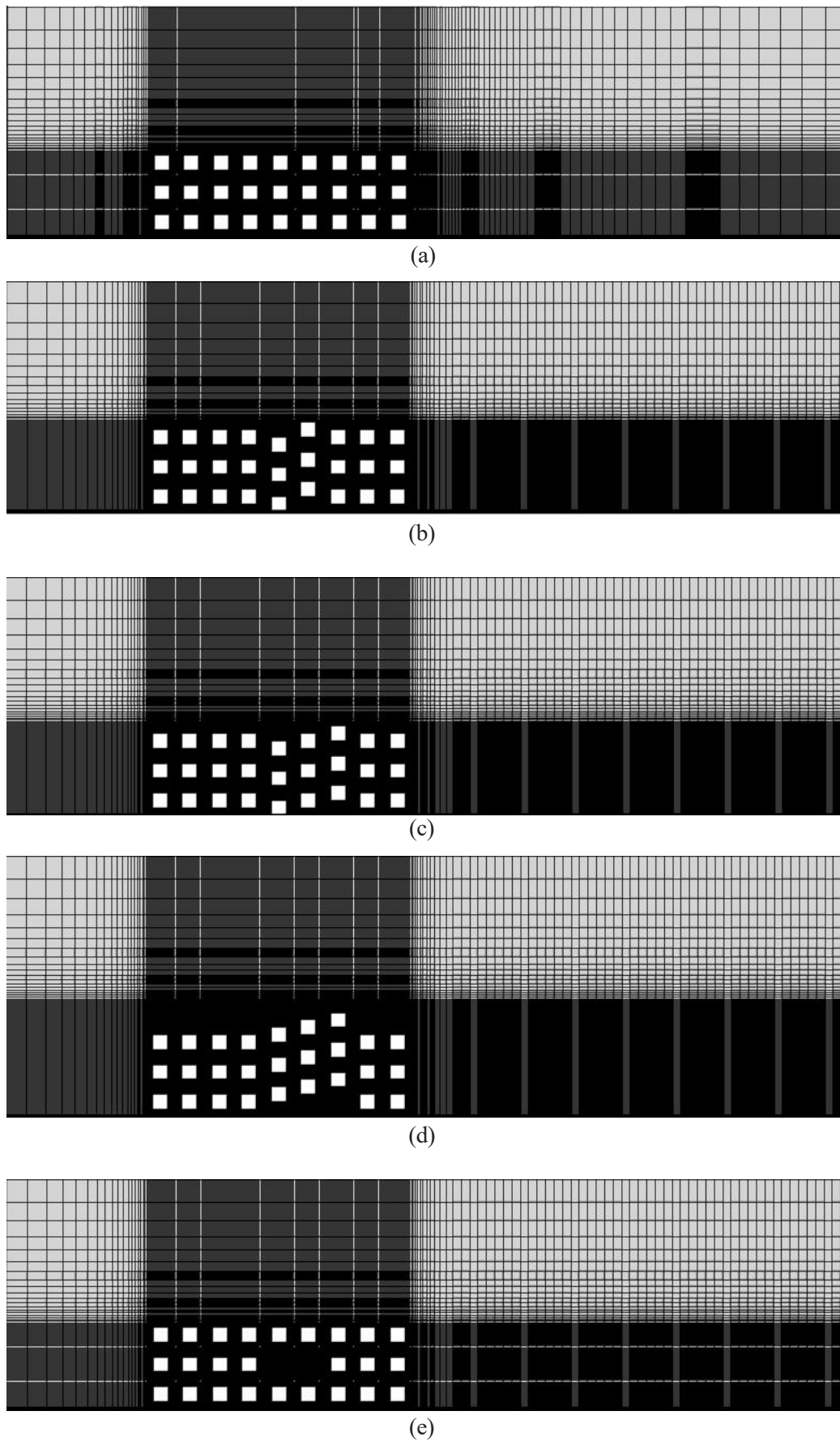
Fig. 8. Top view of the grid for five cases of building layouts: (a) case A (b) case B (c) case C (d) case D (e) case E

Results and discussion

Impacts of layout on pedestrian level wind comfort

Referring to the definition of wind velocity ratio in Ref. [8], this paper employs $R_{1.5}$ to evaluate the pedestrian level wind comfort. $R_{1.5}$ is defined as follows:

$$R_{1.5} = U_{1.5}/U_a \qquad (10)$$

Where $U_{1.5}$ stands for the wind speed of any position at the height of 1.5m above the ground in the building group, and U_a is the inlet velocity at the same height upstream of the building group. In this paper, U_a is 2m/s according to Eq. 8. The index $R_{1.5}$ can reflect the influence of building group on the strength of wind speed. The reason for choosing 1.5m is that this height is not only within the range of human activity but also within the zone of human respiration. The pollutant concentration at the height is discussed in the next session.

Table 1 shows the grades of wind comfort based on the range of $R_{1.5}$. With the increase of $R_{1.5}$, the grade changes from G1 to G5. According to Ref. [9], The threshold value 1.5m/s is the minimum noticeable wind velocity for human, while 5m/s is the highest acceptable mean velocity set in pedestrian level wind comfort criterion [1].The median of G3 is 1.5m/s, so G3 is set as the lowest grade meeting the wind comfort requirement. G1 and G2 are regarded as the levels not conforming to the requirement, while G4 and G5 are higher levels since they meet the requirement of wind comfort and provide good body feeling for pedestrians. Obviously when U_a varies, the lowest grade should changes accordingly.

Fig. 9 shows $R_{1.5}$ and streamline distributions at pedestrian level. Due to the shielding effect of the upstream buildings, the wind speed outside the target area increases, and flow is introduced into the building group. In case A, the introduced flow weakens when it reaches B_{i2}. The wind comfort grade is G1 and G2 near the B_{i1} and B_{i2} while the grade increases to G3 near B_{i3}. Generally the wind comfort grade is lower for most area of case A. The flow and grade of case E is roughly the same as that of Case A, though buildings B_{22} and B_{32} are removed (see Fig. 9 (a) and (e)).

Table 1. Wind comfort grade

Grade name	$R_{1.5}$
G1	(0,0.3]
G2	(0.3,0.6]
G3	(0.6,0.9]
G4	(0.9,1.2]
G5	(1.2,1.5]
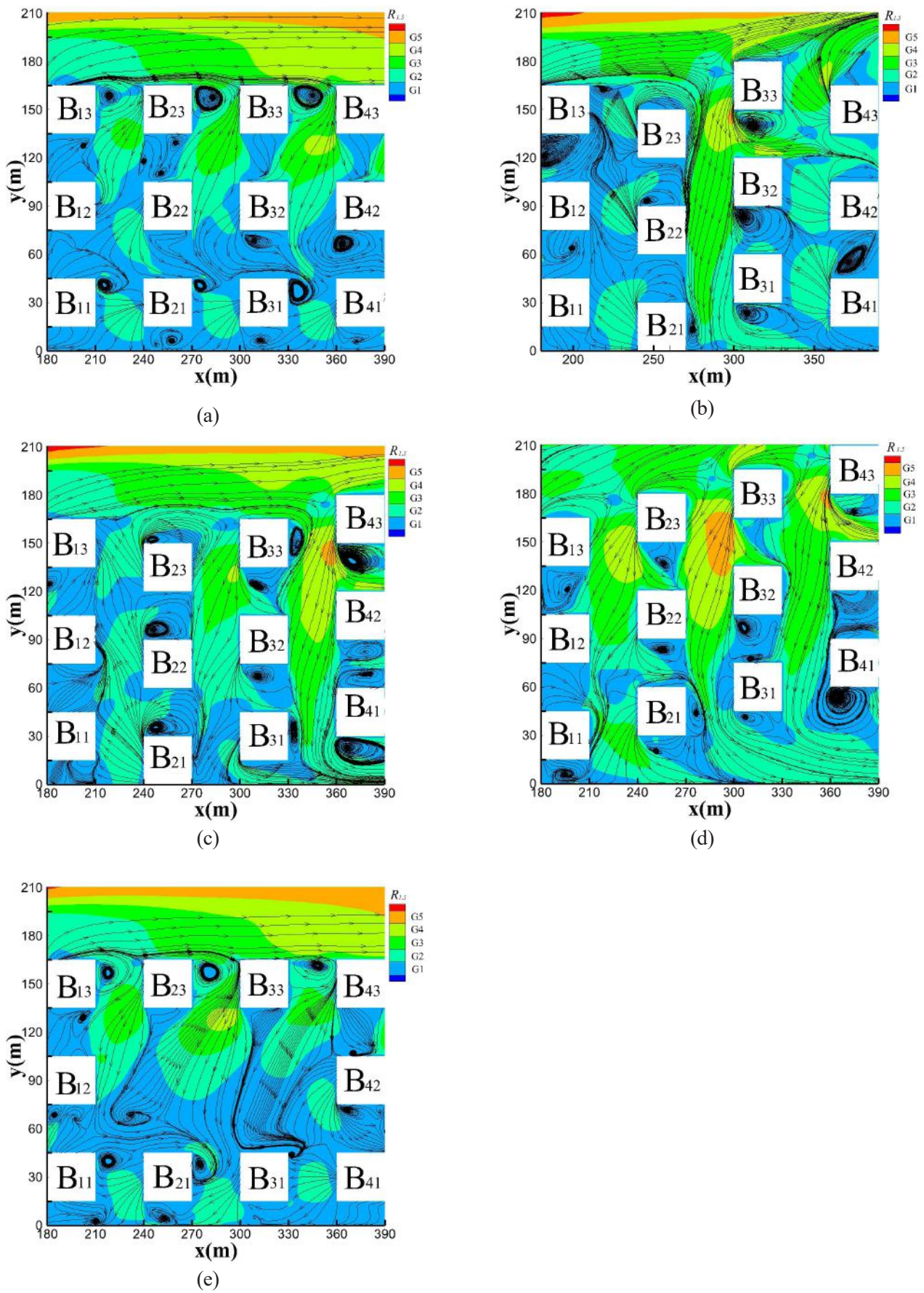
Fig. 9. Distribution of R$_{1.5}$ and streamline at pedestrian level: (a) case A, (b) case B, (c) case C, (d) case D, (e) case E

In the target area, when the downstream buildings is staggered outward along the +y direction relative to the adjacent upstream buildings, the flow introduced into the building group from the outside becomes stronger (see Fig. 9 (b), (c) and (d)). This is the most evident in Case D, in which B_{2j}, B_{3j} and B_{4j} moves in +y direction in succession. Consequently about one half of the area in Case D is labeled with G3 or higher. In case C, B_{3j} and B_{4j} are staggered outward in +y direction relative to B_{2j} and B_{3j} respectively, resulting in slight improvement of wind comfort grade compared with that of case A. In case B, the outward staggered distance between B_{2j} and B_{3j} increases to H, which leads to the local wind comfort grade a little higher. However, the general grade of case B is worse than that of case C.

Fig. 9 also shows that when the downstream buildings are staggered inward along -y direction relative to the upstream buildings, the flow outside the target area cannot enter the building groups. Instead the flow in the region goes out. This can be seen in Fig. 9 (b) and (c).

The above analysis shows that appropriate staggered layout of the building group increases the wind speed and brings higher level of wind comfort grade. In this paper, case D is the best layout while case A and E are the worst for their low wind speed in the target area.

Impacts of layout on pedestrian level concentration

Referring to the definition of dimensionless concentration in Ref. [15], this paper uses K to assess the pollutant level. K is defined as follows:

$$K = \frac{\rho_{co} C Q_{\infty}}{M_0} \tag{11}$$

Where ρ_{CO} is the density of CO (1.25 kg/m^{-3}, under normal temperature and pressure), c is the volume fraction of pollutant, Q_{∞} is the reference flow rate, which is the integral of inlet velocity on the plane obtained by projecting the building group to the inlet surface of the computation domain.

Fig. 10 shows K contours at pedestrian level.

Obviously the pollutants mainly accumulate around B_{1j}, which is next to the pollution source. In the vicinity of the B_{3j} and B_{4j}, K is negligible. In terms of the area with K >20, Case B and case C have larger values than other cases. In case D, K is maintained below 20 on most part of the target area, and the maximum of K, which is about 50, is the lowest in five cases. So case D is least affected by upstream pollutants. The distribution of K in case A and case E are similar, and their area with K >20 is larger than that of case D but smaller than that of case B.

In fact, the K distribution is closely related with the wind field between B_{1j} and B_{2j}. Comparing Fig.9 with Fig.10, it can be found that the flow in -y direction between B_{1j} and B_{2j} prevents diffusion of pollutants from the source. Particularly in case D, the outward staggered arrangement creates the strongest flow in -y direction, thus resulting in the lowest pollutant concentration. While in case B and case C, the inward staggered arrangement of B_{2j} reverses the flow and weakens the wind speed, thus leading to pollutant accumulation near B_{1j}. In the non-staggered case A and case E, the flows in -y direction disappear at the corner of B_{12}, so the value of K between B_{1j} and B_{2j} increases gradually along -y direction.

In addition to the influence of convection, the turbulent diffusion also plays a role in pollutant distribution. Fig. 11 shows the turbulent intensity (TI) at pedestrian level. The area with high TI is the largest in case D, which contributes to keeping the pollutant concentration low by turbulent diffusion. However the TI between B_{13} and B_{23} in case B and case C is less than 10%, leading to weak diffusion of the local pollutant. Therefore K is relatively large between B_{13} and B_{23} of the two cases.

Fig. 11 also shows that at the sharp corners of the outward staggered buildings, TI is greater than 20%, such as B_{33} in case B, B_{43} in case C, B_{23}, B_{33}, and B_{43} in case D. At the same time the strength of TI is also consistent with the velocity value. Comparing Fig.10 with Fig. 11, it can be seen that the area with higher wind speed is also covered with higher TI.
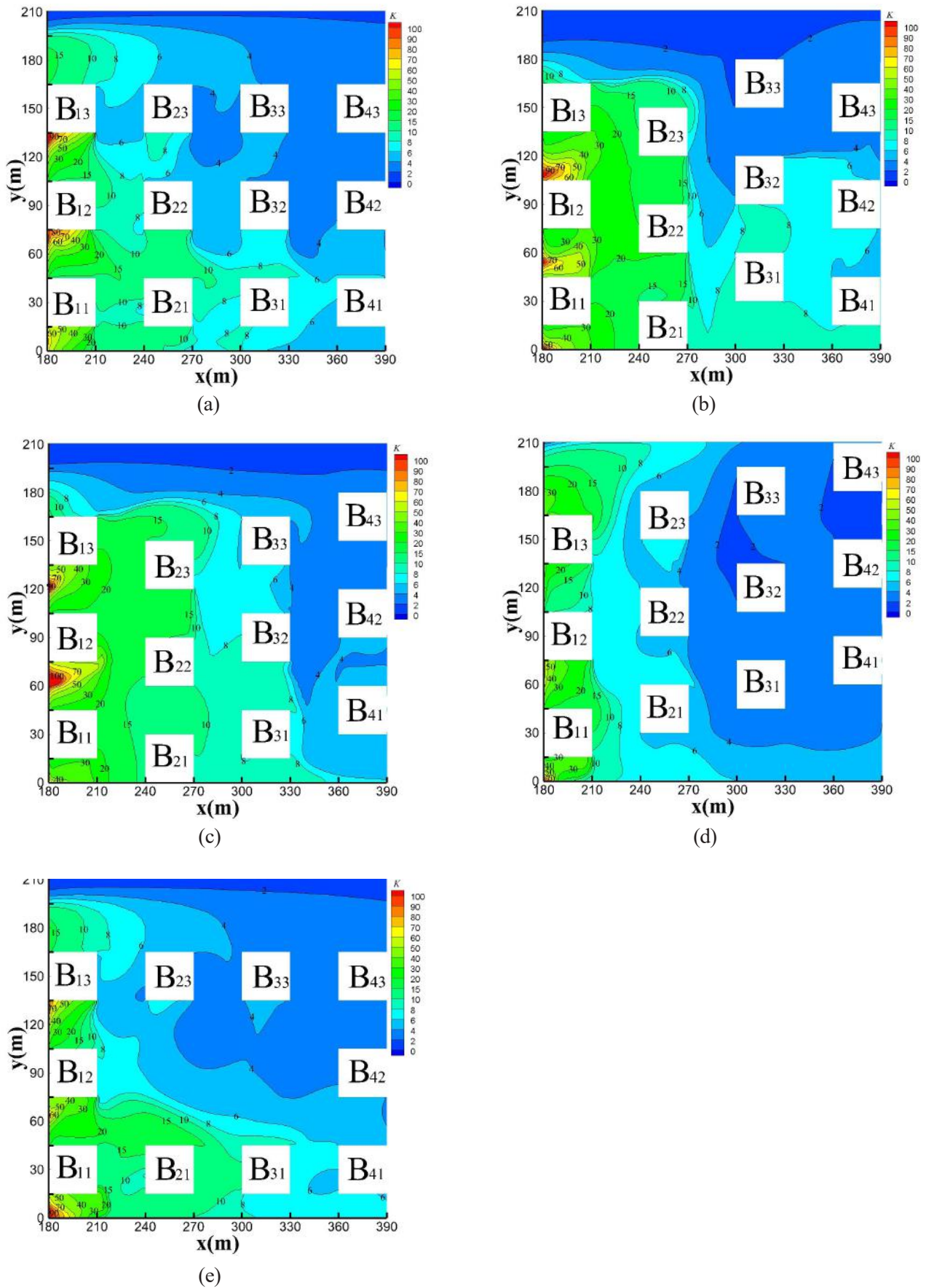
Fig. 10. Distribution of K at pedestrian level: (a) case A, (b) case B, (c) case C, (d) case D, (e) case E
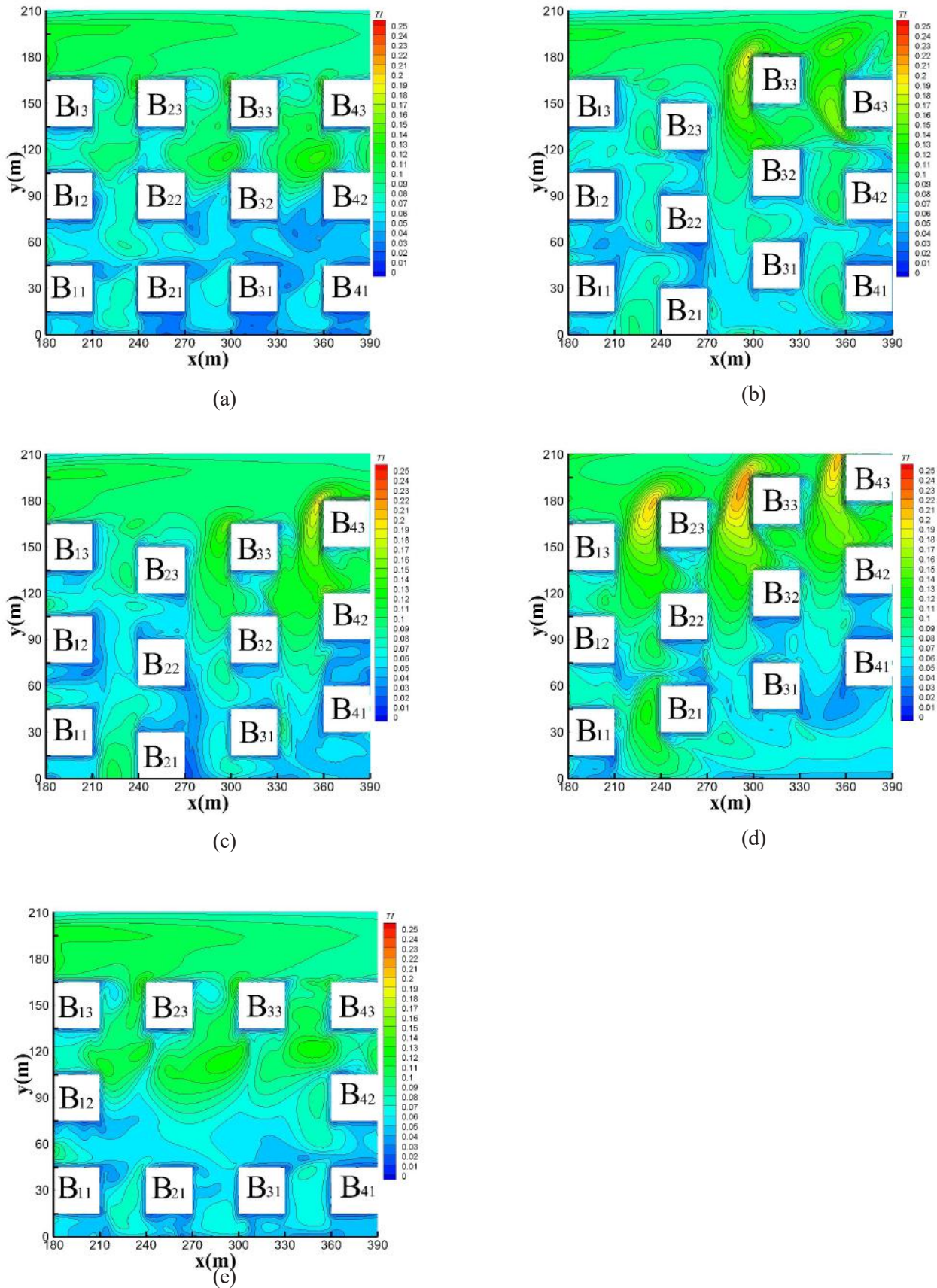
Fig. 11. Distribution of turbulent intensity at pedestrian level: (a) case A, (b) case B, (c) case C, (d) case D, (e) case E

Conclusion

The CFD method in this paper is validated according to the wind tunnel experimental data. The impacts of building layouts on flow and pollutant diffusion are numerically investigated using the standard k-ε turbulence model. The wind comfort grade and pollutant concentration at pedestrian level are assessed by normalized parameters of $R_{1.5}$ and K respectively. The outward staggered layout of building can improve both wind comfort grade and air quality, but the inward staggered layout has the adverse effect. The wind comfort grade of non-staggered layouts is the lowest in this paper. The study reinforces the importance of optimizing the building layout to maintain a livable outdoor environment.

Financial supports

Competing interests

The authors declare that there are no competing interests.

Acknowledgements

Ethical considerations

Ethical issues (Including plagiarism, Informed Consent, misconduct, data fabrication and/or falsification, double publication and/or submission, redundancy, etc.) have been completely observed by the authors.

References

1. Blocken B, Stathopoulos T, Beeck JP. Pedestrian-level wind conditions around buildings: Review of wind-tunnel and CFD techniques and their accuracy for wind comfort assessment. Building and Environment. 2016 May 1;100:50-81.

2. Toparlar Y, Blocken B, Maiheu B, Heijst GJ. A review on the CFD analysis of urban microclimate. Renewable and Sustainable Energy Reviews. 2017 Dec 1;80:1613-40.

3. Stathopoulos T. Pedestrian level winds and outdoor human comfort, Journal of Wind Engineering and Industrial Aerodynamics. 2006 Nov 1;94(11):769-80.

4. Mittal H, Sharma A, Gairola A. A review on the study of urban wind at the pedestrian level around buildings. Journal of Building Engineering. 2018 Jul 1;18:154-63.

5. Shui T, Liu J, Yuan Q, Qu Y, Jin H, Cao J, Liu L, Chen X. Assessment of pedestrian-level wind conditions in severe cold regions of China. Building and Environment. 2018 May 1;135:53-67.

6. Liu J, Niu J, Du Y, Mak CM, Zhang Y. LES for pedestrian level wind around an idealized building array—Assessment of sensitivity to influencing parameters, Sustainable Cities and Society. 2019 Jan 1;44:406-15.

7. Mittal H, Sharma A, Gairola A. Numerical simulation of pedestrian level wind flow around buildings: Effect of corner modification and orientation. Journal of Building Engineering. 2019 Mar 1;22:314-26.

8. Du Y, Mak CM. Effect of lift-up design on pedestrian level wind comfort around isolated building under different wind directions. Procedia Engineering. 2017 Jan 1;205:296-301.

9. Du Y, Mak CM, Liu J, Xia Q, Niu J, Kwok KC. Effects of lift-up design on pedestrian level wind comfort in different building configurations under three wind directions. Building and Environment. 2017 May 15;117:84-99.

10. Chew LW, Norford LK. Pedestrian-level wind speed enhancement in urban street

canyons with void decks. Building and Environment. 2018 Dec 1;146:64-76.

11. An K, Wong SM, Fung JC. Exploration of sustainable building morphologies for effective passive pollutant dispersion within compact urban environments. Building and Environment. 2019 Jan 15;148:508-23

12. Bijad E, Delavar MA, Sedighi K. CFD simulation of effects of dimension changes of buildings on pollution dispersion in the built environment. Alexandria Engineering Journal. 2016 Dec 1;55(4):3135-44

13. Sha C, Wang X, Lin Y, Fan Y, Chen X, Hang J. The impact of urban open space and 'lift-up' building design on building intake fraction and daily pollutant exposure in idealized urban models. Science of The Total Environment. 2018 Aug 15;633:1314-28.

14. Chavez M, Hajra B, Stathopoulos T, Bahloul A. Near-field pollutant dispersion in the built environment by CFD and wind tunnel simulations. Journal of Wind Engineering and Industrial Aerodynamics. 2011 Apr 1;99(4):330-9.

15. Hang J, Li Y, Sandberg M, Buccolieri R, Di Sabatino S. The influence of building height variability on pollutant dispersion and pedestrian ventilation in idealized high-rise urban areas. Building and Environment. 2012 Oct 1;56:346-60.

16. Yassin MF. Impact of height and shape of building roof on air quality in urban street canyons. Atmospheric Environment. 2011 Sep 1;45(29):5220-9.

17. Takano Y, Moonen P. On the influence of roof shape on flow and dispersion in an urban street canyon. Journal of Wind Engineering and Industrial Aerodynamics. 2013 Dec 1;123:107-20.

18. Murena F, Mele B. Effect of balconies on air quality in deep street canyons. Atmospheric Pollution Research. 2016 Nov 1;7(6):1004-12.

19. Llaguno-Munitxa M, Bou-Zeid E, Hultmark M. The influence of building geometry on street canyon air flow: validation of large eddy simulations against wind tunnel experiments. Journal of Wind Engineering and Industrial Aerodynamics. 2017 Jun 1;165:115-30.

20. Ai ZT, Mak CM. CFD simulation of flow in a long street canyon under a perpendicular wind direction: Evaluation of three computational settings. Building and Environment. 2017 Mar 1;114:293-306.

21. Zhang YW, Gu ZL, Cheng Y, Lee SC. Effect of real-time boundary wind conditions on the air flow and pollutant dispersion in an urban street canyon—large eddy simulations. Atmospheric Environment. 2011 Jun 1;45(20):3352-9.

22. Yu Y, Kwok KC, Liu XP, Zhang Y. Air pollutant dispersion around high-rise buildings under different angles of wind incidence. Journal of Wind Engineering and Industrial Aerodynamics. 2017 Aug 1;167:51-61.

23. Tominaga Y, Stathopoulos T. CFD simulation of near-field pollutant dispersion in the urban environment: A review of current modeling techniques. Atmospheric Environment. 2013 Nov 1;79:716-30.

24. Fluent Inc, 2010. Fluent 13.0. Theory guide. Fluent Inc, Canonsburg, PA.

25. Tanaka H, Yoshie R, Hu CH. Uncertainty in measurements of velocity and concentration around a building. InProceedings of the 4th International Symposium on Computational Wind Engineering 2006 Jun (pp. 549-552).

26. Tominaga Y, Mochida A, Yoshie R, Kataoka H, Nozu T, Yoshikawa M, Shirasawa T. AIJ guidelines for practical applications of CFD to pedestrian wind environment around buildings. Journal of Wind Engineering and Industrial Aerodynamics. 2008 Oct 1;96(10-11):1749-61.

27. Yu H, Thé J. Validation and optimization of SST k-ω turbulence model for pollutant dispersion within a building array. Atmospheric Environment. 2016 Nov 1;145:225-38.